Journal of Asian Concrete Federation
Vol. 6, No. 2, pp. 1-13, December 2020
ISSN 2465-7964 / eISSN 2465-7972
https://doi.org/10.18702/acf.2020.12.6.2.1

Technical Paper

Mechanical characterization of a FRCM system with aramid fiber fabric embedded in green high-strength cementitious matrix

Munkhtuvshin Ochirbud, Donguk Choi*, Undram Naidanjav, S.-S. Ha, C.-Y. Lee

(Received August 13, 2020; Revised October 26, 2020; Accepted October 28, 2020; Published December 31, 2020)

Abstract: Fabric reinforced cementitious matrix (FRCM) system can be applied to strengthen existing RC structures. In this experimental study, aramid fiber (AF) mesh was used along with green high-strength mortar (f'_c = 75.6 MPa) incorporating fine waste glass powder as partial replacement of cement and 100% recycled fine aggregate. Test objective was to provide basic design parameters through mechanical characterization of the AF-FRCM system. Three different types of tests were conducted: Uniaxial test of tensile specimens; flexural test of composite short beams; and pull-off test of thin FRCM placed on top of normal strength concrete. Thickness of FRCM was about 10 mm while the volumetric ratio of the fiber fabric to gross volume was 1.3% (0.65% in each direction). Tensile test results showed that the load-displacement relationship of the FRCM was relatively ductile, while tensile behavior of the AF governed at the peak load. Nominal tensile strength of the FRCM cross-section was 6.4 MPa at 4.6% strain of the composite material. Short beam strength of 1.3 MPa was determined from flexural test of composite short beams (or interlaminar shear test) performed following ASTM D2344M. In the pull-off test, two different failure modes were identified: Interface failure or substrate failure in tension. Average pull-off strength was 2.84 MPa. Design values were suggested based on current test results of the AF-FRCM.

Keywords: FRCM; aramid fiber; green high-strength mortar; tensile test; composite short beam; pull-off test.

1 Introduction

Fabric-reinforced cementitious matrix (FRCM) system is a relatively new technology in the area of strengthening and repair of RC and masonry structures. Externally-bonded FRCM system typically consists of one or more layers of 2D or 3D fiber fabric and the cementitious matrix in which the fiber fabric is embedded. The performance of the FRCM system at elevated temperatures is significantly enhanced compared to that of the external fiber reinforced polymer (FRP) strengthening as the fiber fabric is protected in the inorganic cementitious matrix [1]. The FRCM technology is applicable to wet surface. As the fibers are not directly exposed to outdoor environment, the fiber fabric is prevented from outdoor weathering such as ultra violet exposure. The FRCM technology has originally evolved from the ferrocement, where the metallic reinforcement is replaced by fabrics of dry fibers [2].

Research performed to define mechanical properties of the FRCM system and develop more efficient technology to strengthen RC members have been active during the last decade. Existing studies on the mechanical characterization of the FRCM system include tensile behavior of the FRCM, bond and/or pull-off behavior of FRCM bonded to concrete, and interlaminar shear behavior [3-10]. Many researchers concentrated on the behavior of the FRCM-strengthened RC members such as flexural

Munkhtuvshin Ochirbud *is a M.S. student of the School of Architecture, Hankyong National University, South Korea.*
Corresponding author Donguk Choi *is a Professor in the School of Architecture & Design Convergence, Hankyong National University, South Korea.*
Undram Naidanjav *is a M.S. student of the School of Architecture, Hankyong National University, South Korea.*
S.-S. Ha *is a Professor of the Divison of Real Estate and Construcion Engineering, Kangnam University, South Korea.*
C.-Y. Lee *is a Principal Researcher and CEO of CareCon, Ltd, South Korea.*

and shear strengthening of RC beams as well as confinement of concrete columns [11-19]. Ebead and El-Sherif studied the behavior of RC beams strengthened in flexure using near surface embedded-FRCM [20]. It is noted that the FRCM can be an efficient technology to repair historic structures such as arches and vault as it is applicable on the curved surface [21].

Although the performance of many different fibers has been investigated such as carbon fiber, glass fiber, basalt fiber, or polyparaphenylene benzobisoxasole (PBO) fiber, there are still few published results of research on the mechanical characterization of aramid fiber fabric embedded in cementitious matrix. Caggegi et al. investigated the tensile properties of uniaxial aramid textile and quadriaxial aramid textile fabric [22]. Due to dense textile of aramid fibers, cementitious matrix delaminated during tensile testing and hence low fiber stress of 1,089 MPa at ultimate was reported for the uniaxial aramid textile. Higher ultimate strength of the aramid fiber of 1,354 MPa was shown by the quadriaxial textile where the aramid fabric slippage was observed from the cementitious matrix. In another investigation by Ascione et al., coated bidirectional glass-aramid fiber textile was tested [23]. The glass-aramid textile showed 1,784 MPa strength of the fiber in tension at ultimate. In this test, due to use of hydraulic grip of the UTM which restrained the free slippage of the fabric from the cementitious matrix during tensile test, the final failure mode was rupture of the glass-aramid fibers at 2.02% strain.

In this study, aramid fiber (AF) was used in a form of 2D fabric (AF mesh) along with a green high-strength mortar utilizing recycled materials such as finely ground waste glass powder and recycled fine aggregate. Three different experimental programs were carried out: Uniaxial test of FRCM tensile specimens, flexural test of composite short beams made of double FRCM layers following ASTM D2344M, and pull-off test using FRCM-concrete blocks [24]. The purpose was to provide basic design parameters and the rational mechanical characterization of the AF-FRCM system. It is noted that the cementitious matrix (mortar) used in this study is of significantly higher strength than low-to-medium strength mortars often used for FRCM [8]. Use of a high-strength mortar was deemed necessary to increase the tensile capacity of the AF-FRCM system. As the binder content increases with use of the high-strength mortar, fine waste glass powder was used to partially replace cement. Recycled fine aggregate was also used to replace natural sand, considering economical aspect of the AF-FRCM system as well as to promote sustainability.

2 Experimental program

2.1 Materials

2.1.1 Aramid fiber mesh

Aramid fiber roving (1100 Dtex) was used to fabricate the AF mesh in the laboratory where the warp spacing and the weft spacing was 11.25 mm and 22.5 mm on center, respectively, as shown in Fig. 1. Longitudinal and transverse fibers were bonded together using an adhesive at each junction. Table 1 shows the physical and mechanical properties of the AF roving determined in this study following ISO 10406-2 [25]. Thickness of a fiber roving was about 1.86 mm and AF covered about 24% of the surface (i.e. surface area of AF to gross area ≅ 24%). The AF roving has 2,331 MPa tensile strength at 3.74% strain as shown in Table 1. The AF demonstrated a linearly elastic stress-strain relationship until failure in tension.

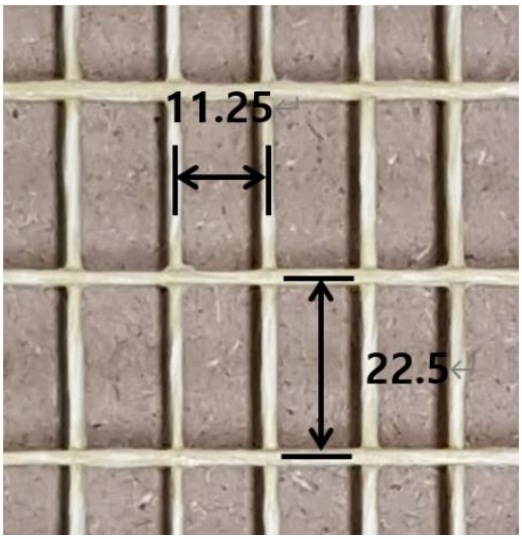

Fig. 1 – AF mesh

Table 1 – Physical and mechanical properties of AF roving

Cross-sectional area (mm^2)	0.737
Density (g/mm^3)	0.00144
Strength, f_{fu} (MPa)	2,331
Ultimate strain, ε_{fu}	0.0374
Elastic modulus, E_f (GPa)	61.4
Coefficient of thermal expansion (m/m/℃)	-2.4×10^{-6}

NOTE: Results of 12 tensile tests of AF roving, where density and coefficient of thermal expansion were supplied by manufacturer.

2.1.2 Green high-strength cementitious matrix

A high-strength cementitious matrix for the FRCM system was necessary because the FRCM technology was to be used for the purpose of strengthening RC members after the current phase of study. As the material cost of the high-strength cementitious matrix increases due to use of silica fume (SF) and siliceous sand in large quantities, it was determined to introduce recycled materials as constituents such as fine waste glass powder (WGP) and recycled fine aggregate (RFA) [27]. While there are several types of the waste glass powders used in Korea such as those produced from LCD waste glass, green or brown glass bottles, plate glass, the WGP used in this study was manufactured by crushing and grinding waste green bottles. The finely ground WGP (< 50 μm) is an amorphous material with more than 78% silica content. Table 2 shows the mix design of the green high-strength mortar used in this study, where WGP partly replaces SF in Table 2. Sand used was 100% RFA produced from demolished concrete. The wet-processed RFA was supplied by a commercial producer. The maximum particle size was 2.5 mm. Figure 2 shows gradation of cement, SF, WGP, and RFA. Polycarboxylic acid base superplasticizer (SP) by 1 wt.% of total binder was used to control flow. Flow of the fresh mortar measured following KS L 5105 was 24.2 cm as shown in Table 2 [28]. The compressive strength of the mortar was determined by testing three 50 mm × 50 mm × 50 mm cubes at 7, 28, and 56 days, respectively. Flexural strength was determined by testing two 40 mm × 40 mm × 160 mm beams under three points loading in flexure 28 days after casting. Density and voids of the hardened mortar were determined following ASTM D642 after 28 days [29].

RFA produced from multi-stage crushing and sieving process of demolished concrete and satisfying requirements of KS F 2527 was used [30]. When the RFA replaces the natural sand, due to adhered mortar of the recycled aggregate particles, which absorbs and releases water easily, the mortar with RFA can experience higher shrinkage than the mortar with natural sand [31]. Shrinkage behavior of the green mortar was monitored for 90 days. Three 40 mm x 40 mm x 160 mm mortar bars were cast. After demolding on the next day, the mortar bars were immediately brought to an environmental chamber where the relative humidity and temperature were maintained at 60±5% and 20±2℃, respectively. Length change of each mortar bar was monitored using a dial gauge with 0.05 mm accuracy.

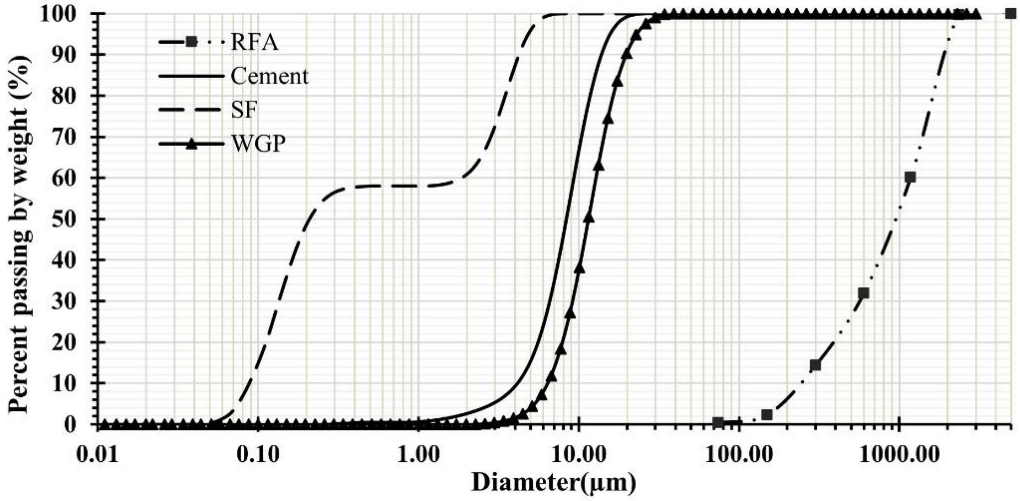

Fig. 2 – Gradation of cement, silica fume, waste glass powder and recycled sand

Table 2 – Mix design for green high-strength mortar and flow of fresh mortar

C (kg/m^3)	SF (kg/m^3)	WGP (kg/m^3)	RFA (kg/m^3)	W (kg/m^3)	w/b	SP (kg/m^3)	Flow (cm)
550	27.5	110	1,487	206	0.3	6.88	24.2

NOTE: Density of C, SF, WGP, RFA is 3.15, 2.2, 2.5, 2.47, respectively; water absorption of RFA is 2.34% in oven-dry state.

2.2 Test method

2.2.1 Tensile test of FRCM

A thin FRCM plate (width = 405 mm, height = 450 mm, thickness ≈ 10 mm) was fabricated. AF mesh that consisted of one fiber roving at 11.25-mm center-to-center spacing (warp) and two fiber rovings at 22.5-mm spacing on center (weft) was first installed at half-depth of the 10-mm-thick plate, and then the green high-strength mortar was cast to full depth. The thin plate was wet cured until test date. Nine 45-mm-wide and 450-mm-long FRCM flat bars were cut from the plate using waterjet 28 days after casting. Two specimens cut from both sides of the plate were used for preliminary tests, and therefore a total of seven tensile test specimens was retained for the tensile tests. The tensile test started 56 days after casting. One week prior to testing, a set of two rectangular 6-mm-thick steel plates was bonded to each end of the tensile test specimen on both sides using two-part epoxy. The behavior of 120-mm length in the middle was monitored during the tensile test. The tensile test was performed under displacement control at a rate of 1 mm per minute using Instron 4495 universal testing machine (UTM). Figure 3 schematically shows the specimen fabrication method and the testing configuration. A set of extensometer with 100-mm gauge length was used to measure longitudinal strains developed in the mid-part of a specimen as shown in Fig. 3(b). Test data were electronically monitored and saved using a TDS 530 data logger and a notebook PC.

2.2.2 Flexural test of composite short beams

The flexural test of composite short beams (or interlaminar shear test) specimens were fabricated following ASTM D2344M, which recommends that [24]:

(a) Specimen length = thickness × 6
(b) Specimen width = thickness × 2

To fabricate flexural test specimens, a mold for 20-mm-thick FRCM plate (width = 405 mm, height = 225 mm) was prepared. Two layers of AF mesh was installed in the mold, where the first and the second AF mesh plane was at 5-mm and 15-mm depth, respectively. Green high-strength mortar was cast in two shifts of equal thickness of about 10 mm each. The bottom layer was cast first followed by the top layer three days after casting the bottom layer without any surface treatment. Nine 45-mm-wide and 225-mm-long double-layered beams were cut out from the plate by waterjet 28 days after casting the first layer. 52.5-mm length from each end of the beam was cut off using a masonry saw. Two beams cut from both sides of the plate were used for the preliminary tests. Finally, seven composite short beams

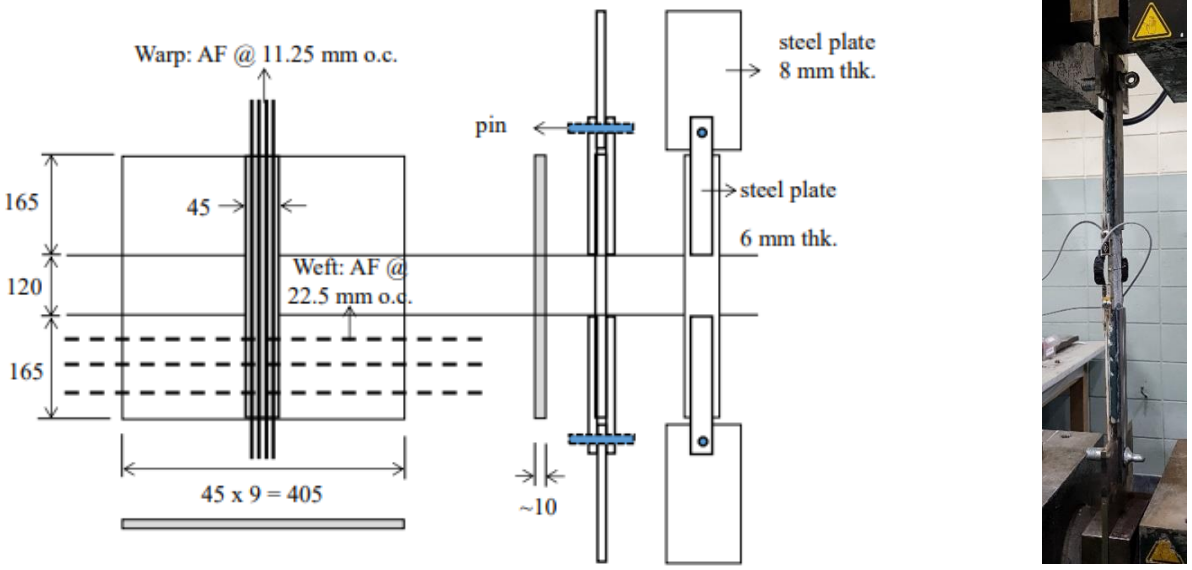

(a) Specimen fabrication and setup for tensile test (unit: mm)

(b) Test in progress

Fig. 3 – Tensile test

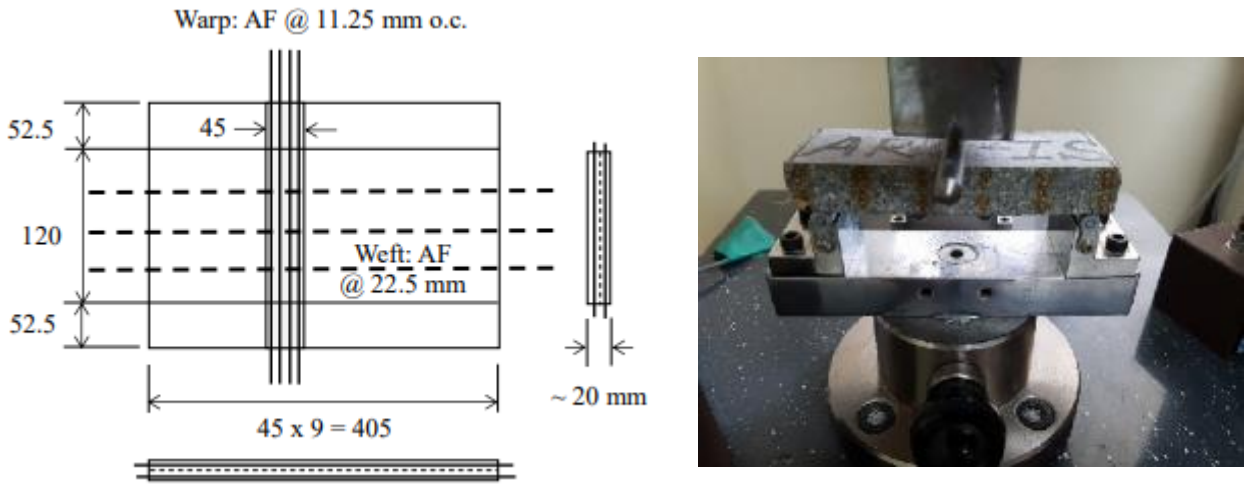

(a) Schematics of specimen fabrication (unit: mm) (b) Test under progress

Fig. 4 – Flexural test of composite short beams

were used toward the flexural tests: Each beam was about 120 mm long, 45 mm wide, and consisted of double layers of FRCM with equal depth of 10 mm each: i.e., total thickness was about 20 mm (See Fig. 4). The composite beams were tested under three points loading.

The short-beam strength was determined using Eq. (1) as suggested by ASTM D2344M [24]:

$$F^{sbs} = 0.75 \times \frac{P_{max}}{b \text{ x } h} \quad (1)$$

where F_{sbs} is short-beam strength (MPa), P_{max} is maximum load observed during test (N), b = measured specimen width (mm), and h is measured specimen thickness (mm).

Figure 4 shows schematics of the specimen fabrication and the flexural test setup for composite short beams. The flexural test was performed under displacement control at a ramp rate of 1 mm per minute using a 50-kN UTM. Test data were electronically monitored and saved. Load, displacement, failure modes, and crack patterns were carefully observed during and after test.

2.2.3 Pull-off test

For the pull-off test, a 500 mm × 500 mm × 100 mm normal strength concrete block (f_c' = 30 MPa) was first cast. After 28 days, top surface of the concrete block was roughened using two different methods: sand blasting and shot blasting. The sand patch method following ASTM STP763 was used to measure the roughness, which revealed that the average depth of the roughened surface was 0.69 mm and 0.76 mm, respectively, for the sand blasting and

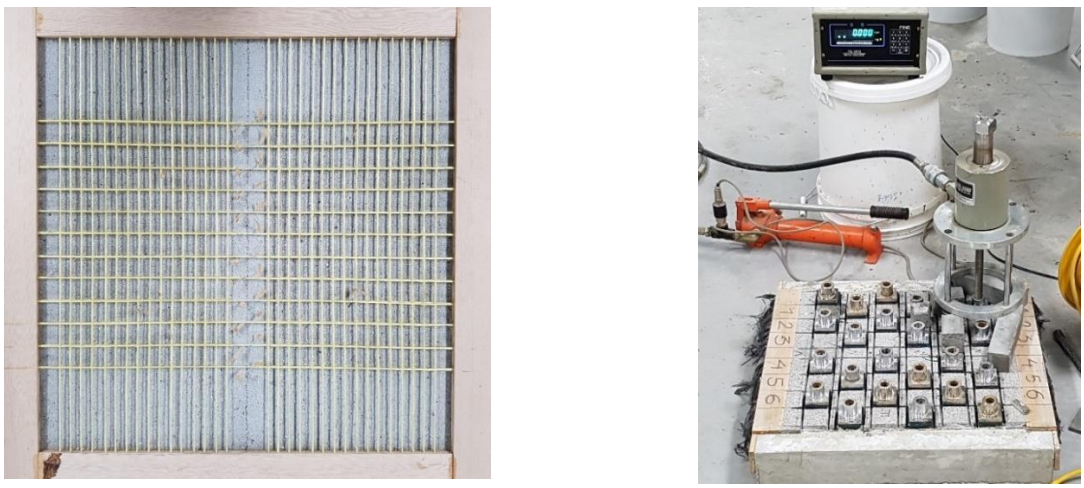

(a) AF mesh installed on top of concrete block prior to mortar casting (b) Pull-off test in progress

Fig. 5 – Pull-off test

shot blasting [32]. After the sand/shot blasting was completed, 3.5-mm thick, 50-mm wide, and 500-mm long hardwood sections (wood plates) were bonded along perimeters on top of the concrete block using adhesive. AF mesh was manually installed using the AF rovings at 11.25-mm center-to-center spacing in one direction and at 22.5-mm spacing on center in the other direction. After the AF mesh was installed, the second layer of 3.5-mm thick hardwood sections were bonded on top of the existing hardwood sections using adhesive so that the total height of the two-layers of hardwood sections plus the AF mesh (at mid height in between the two hardwood layers) altogether was about 8 mm (See Fig. 5(a)). Then green high-strength mortar was cast in one shift. The concrete block with FRCM overlay was consolidated using a vibrating table. The FRCM system was wet cured until test which commenced after 28 days. One week before testing, using a hand grinder, the FRCM overlaid on the concrete block was cut in 45 mm x 45 mm grid pattern as shown in Fig. 5(b). Depth of the cutting was about 25 mm. A steel end plate (40 mm x 40 mm) was bonded to the top surface of the FRCM using two-part epoxy. A pull-off testing apparatus was connected to the steel end plate after allowing the epoxy to develop full strength for one week. To avoid any possible interference between adjacent pull-off tests, a checker board testing pattern was adopted as shown in Fig. 5(b). The maximum load was recorded and the failure mode was observed and recorded.

3 Test results

3.1 Properties of green cementitious matrix

When tests for the mechanical characterization started at 56 days, average compressive strength of three cubes was 75.6 MPa. Average flexural strength determined from flexural test of two mortar bars was 5.50 MPa at 28 days. Density and voids of the hardened mortar were determined following ASTM D642 after 28 days as shown in Table 3 [29]. It is noted that the water-to-binder (w/b) ratio of 0.3 shown in Table 3 does not include free water available from superplasticizer (the sp consists of 30% solid and 70% water by wt.). Including the content of free water available by addition of the sp, the effective water-to-bonder ratio is 0.365, which explains a relatively large voids of 17.6% in Table 3. Figure 6 shows the measured total shrinkage of the three shrinkage test specimens. Figure 6 shows some scatter in the measured total shrinkage versus time curves. Most of the measured shrinkage for 90 days occurred during the first three weeks after casting which is 80.3%, 83.7%, and 85.0% of the 90-day shrinkage, respectively, for each specimen after three weeks. The average total shrinkage strain is 717 μm/m after 90 days.

ACI 209R (1992) technical report suggests an ultimate shrinkage value of 780 μm/m with a correction coefficient of 0.72 for the shrinkage estimation after 3 months, which results in a shrinkage of 562 μm/m after three months [33]. Current data suggested that the shrinkage increase by using 100% recycled sand can be as much as 27.5% compared to a theoretical estimation.

3.2 Tensile test results

The tensile test of seven FRCM tensile specimens was performed using an Instron UTM under displacement control. While the load was monitored from load cell of the UTM, the displacement was measured using a set of 50-mm linear variable displacement transducers (LVDTs), which monitored movement of the UTM cross head. In addition, a set of extensometers with 100-mm gauge length was attached to the mid-part of the specimen to measure tensile strains of the specimen. The tensile test results are summarized in Table 4. Figure 7 shows the fiber stress-versus-strain plots of all tensile tests.

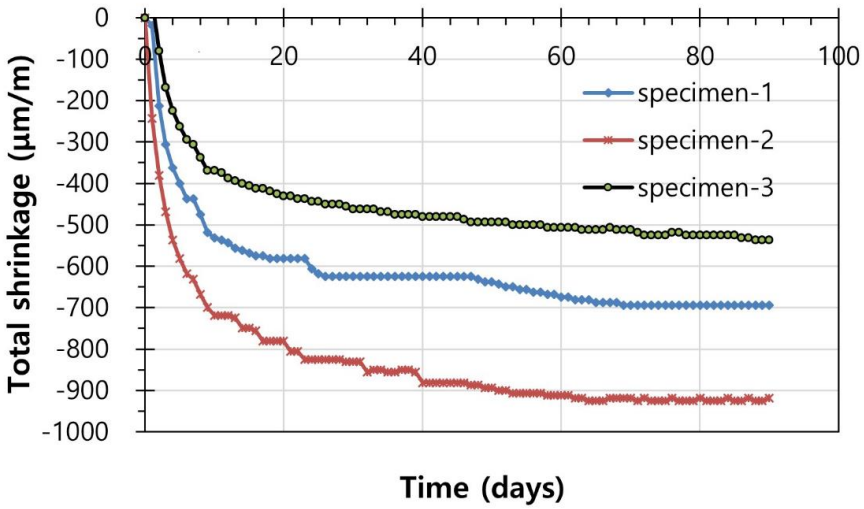

Fig. 6 – Total shrinkage of green high-strength mortar

Table 3 – Properties of hardened mortar

Compressive strength (MPa)			Flexural strength (MPa)	Density (kg/m^3)	Water absorption (%)	Voids (%)
7d	28d	56d				
55.8	71.7	75.6	5.50	2,280	8.37	17.6

Table 4 – Summary of tensile test results

Index	w (mm)	t (mm)	P_{cr} (kN)	P_{max} (kN)	f_f @ P_{max} (MPa)	Displ. @ P_{cr} (mm)	Displ. @ P_{max} (mm)	Average strain @ P_{max}	No. of cracks/ average crack spacing (mm)
AR-T-1	44.05	9.65	0.49	3.08	1,393	0.18	4.85	0.0498	2/45
AR-T-2	44.05	10.55	0.64	3.01	1,361	0.41	5.85	0.0541	3/45
AR-T-3	43.85	11.05	0.73	3.02	1,366	0.17	4.67	0.0400	4/30
AR-T-4	44.15	11.35	0.89	2.71	1,226	0.36	3.36	0.0309	4/30
AR-T-5	43.85	11.05	0.94	2.99	1,352	0.10	4.71	0.0453	3/45
AR-T-6	44.05	10.65	0.52	3.20	1,447	0.17	5.28	0.0509	3/45
AR-T-7	43.95	10.15	0.70	2.90	1,312	0.37	5.13	0.0544	4/30
Average			0.70	2.99	1,351	0.25	4.84	0.0465	
Standard deviation			0.17	0.15	69.1	0.12	0.77	0.0085	
Coefficient of variation			0.24	0.05	0.05	0.49	0.16	0.18	

NOTE: w – width of specimen; t – thickness of specimen; P_{cr} – cracking load; P_{max} – maximum load; average strain = displacement of LVDT divided by 120 mm; no. of cracks – number of tensile cracks developed in the middle 120-mm length of a specimen

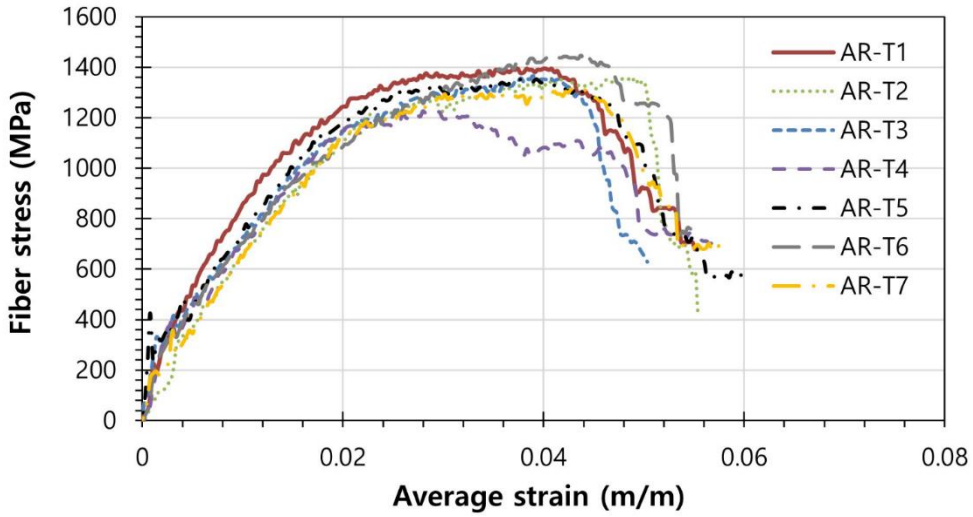

Fig. 7 – Tensile test results: load versus displacement

As the load increased, the first tensile crack appeared within the mid 120-mm length of a test specimen. At the first cracking load P_{cr}, the corresponding tensile stress of the FRCM composite cross-section (i.e. nominal stress) was 1.5 MPa at 0.21% average tensile strain (average of seven tests). As the load further increased, the number of tensile cracks increased. After the number of cracks reached the maximum (2-4 cracks), no new cracks appeared but the existing cracks widened. The tensile cracks typically appeared at position of the lateral fiber roving (weft). Close to the peak load, significant slip of the AF from cementitious matrix was observed adjacent to wide tensile cracks. Test ended when the displacement was 6 mm or greater. In general, the tensile test results indicated a relatively ductile behavior with resistance equal to 6.4 MPa in tension (nominal stress) and 4.6% tensile strain at the peak (average of seven tests). Due to a set of stiff steel plates adhered to both ends of the tensile specimen, the displacement (or strain) of a tensile specimen was dominated by the tensile behavior in the mid part of the specimen (i.e. 120-mm length, See Fig. 3). In Table 4 and Fig. 7, the AF tensile stress at the peak load is 1,351 MPa (average of seven tests) which is only 58% of the fiber tensile strength f_{fu} (See Table 1). The full AF strength in tension was not realized in the current

AF-FRCM system. The average strain at the peak of 4.6% (extensometer) was significantly greater than the AF rupture strain of 3.74%, which indicated that the AF mesh slipped from the cementitious matrix close to the peak load. Figure 9(a) shows load-versus-displacement plots determined from LVDT readings while Fig. 9(b) shows load-versus-strain readings determined from extensometer. The strain values in Fig. 9(b) are smaller than the strain values determined from measured displacements shown in Fig. 9(a) because tensile cracks often developed outside the 100-mm gauge length of the extensometer. As a result, the displacement readings from LVDTs were used to determine average strains shown in Table 4.

3.3 Results of flexural test of composite short beams

Flexural test was performed on seven composite short beams under three point loading. Beam length (measured from support-to-support) was 100 mm for all beams. The flexural test results are summarized in Table 5. Figure 10 shows the cracks developed in a composite beam after test (AR-IS-5). As shown in Table 5 and Fig. 10, all beams show flexural failure rather than shear failure mode.

(a) Before test

(b) After cracking/before peak load

(c) At peak load

(d) Face A after test

(e) Face B after test

Fig. 8 – A tensile test and test results: AR-T-1

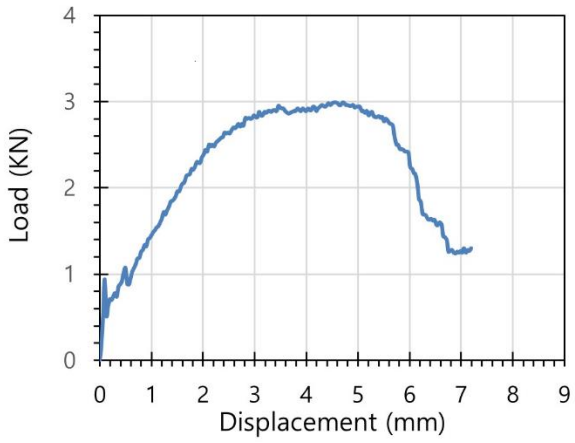

Load-displacement (LVDT)

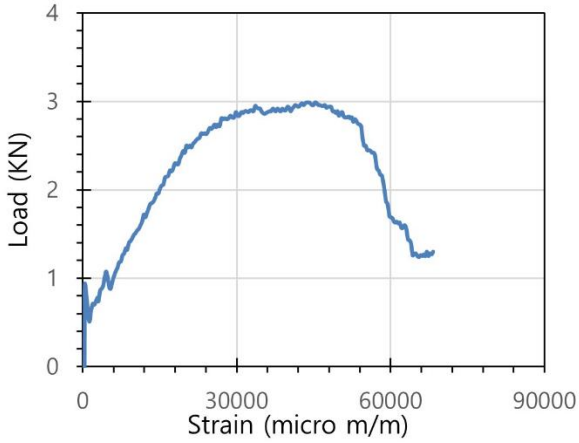

Load-strain (extensometer)

Fig. 9 – Tensile test results of AR-T-5

In all short beams, one or two flexural crack(s) occurred close to the mid-span. Crack(s) gradually progressed beyond the interface and inclined toward the loading point. At ultimate, the concrete crushing at the top compression fiber was observed resulting in a flexural failure. Figure 11 shows the load-versus-mid-span deflection plots of all flexural test specimens. As shown in Fig. 11, the load resisting capacity of the composite beams does not significantly drop after the peak is reached. The flexural test was terminated when the displacement at center was 5 mm or greater.

In Table 5 and Figure 11, the peak loads range between 1.30 kN and 1.51 kN. The peak loads are reached at mid-span displacement between 1.34 mm and 4.46 mm. The short beam strength in Table 5 was determined using Eq. (1). The average short beam strength is 1.30 MPa and the strength ranges between 1.24 MPa and 1.38 MPa.

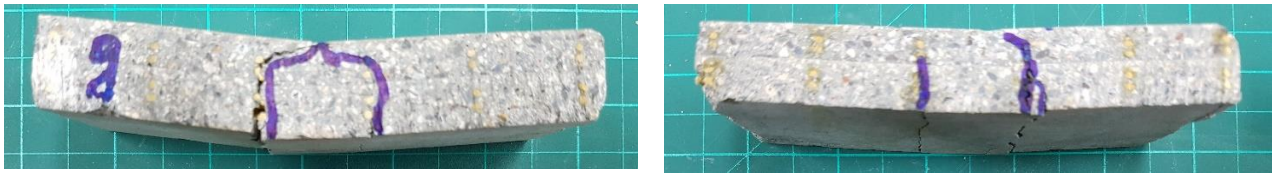

Fig. 10 – Cracks developed after flexural test: AR-IS-5

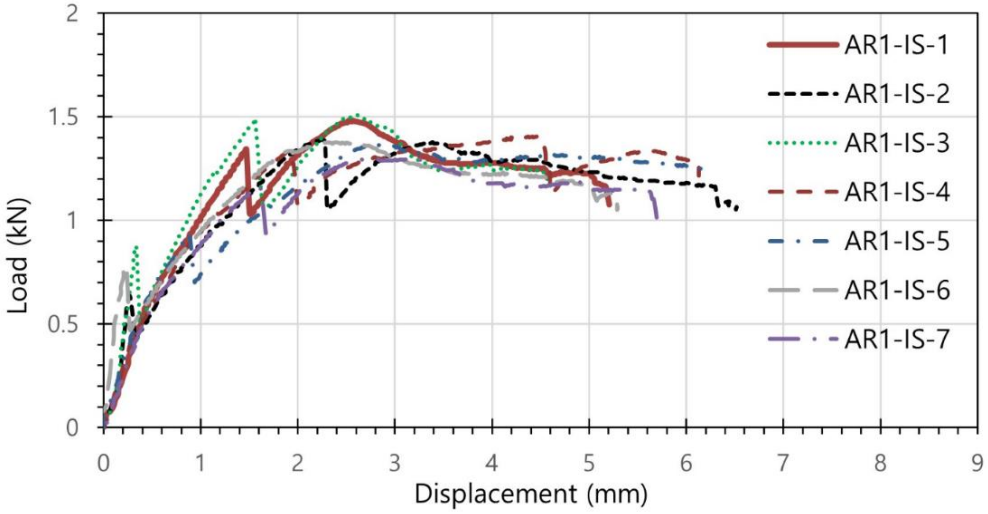

Fig. 11 – Load vs. displacement: flexural test of composite short beams

Table 5 – Summary of flexural test results

Index	Short beam dimensions			Shear span Ratio (a/h)	P_{max} (kN)	Displ. at P_{max} (mm)	Short beam strength (MPa)	Failure mode
	L (mm)	h (mm)	w (mm)					
AR1-IS-1	115.1	18.55	43.85	2.70	1.48	2.56	1.37	flexural failure
AR1-IS-2	114.2	18.20	44.15	2.75	1.39	2.23	1.29	flexural failure
AR1-IS-3	114.0	18.65	44.05	2.68	1.51	2.60	1.38	flexural failure
AR1-IS-4	112.1	18.80	43.95	2.66	1.41	4.46	1.28	flexural failure
AR1-IS-5	113.3	18.80	44.10	2.66	1.37	1.34	1.24	flexural failure
AR1-IS-6	113.6	18.30	44.30	2.73	1.38	1.50	1.27	flexural failure
AR1-IS-7	114.2	17.55	43.95	2.85	1.30	3.13	1.26	flexural failure
				Average	1.40	2.55	1.30	
				Standard deviation	0.07	1.05	0.05	
				Coefficient of variation	0.05	0.41	0.04	

NOTE: L – length of beam; h – height of beam; w – width of beam; a – shear span; P_{max} – maximum load; Displ. at P_{max} – beam mid-span displacement at P_{max}.

3.4 Pull-off test results

The pull-off test was performed using a pull-off testing apparatus as shown in Fig. 5(b). Test results are summarized in Table 6 in terms of peak load, pull-off strength, and failure mode. A total of twelve tests was performed on the shot-blasted and the sand-blasted interfaces, respectively. From the shot-blasted interface, four failures occurred at the interface between the FRCM and concrete (average pull-off strength = 3.25 MPa) while six failures occurred in existing concrete below the interface or substrate (average pull-off strength = 2.99 MPa). From the sand-blasted interface, four failures occurred at the interface (average pull-off strength = 1.62 MPa) while eight failures occurred in the substrate (average pull-off strength = 3.15 MPa). Overall, the pull-off strength of the shot-blasted interface (3.09 MPa) is greater than that of the sand-blasted interface (2.64 MPa). From all pull-off tests, the average pull-off strength is 2.84 MPa.

4 Discussions

The volumetric ratio of the AF mesh to gross volume was 1.3% in this study (or 0.65% in the axial direction). The fiber amount was sufficient so that the fiber tensile behavior governed the tensile behavior of the FRCM system. At P_{max} of 2.99 kN (average of seven tests), the nominal tensile resistance (i.e. P_{max} divided by the gross section) of the FRCM composite section was 6.4 MPa. A characteristic strength (or a design value) can be defined as the average value minus one standard deviation (ACI 549.4R). The peak load was reached at an average strain of 4.65% with standard deviation of 0.85%, resulting in characteristic strain at the peak of 3.8%. Overall the tensile behavior was ductile with relatively good capacity of deformation accompanied by multiple number of clearly visible cracks (two to four cracks over 120-mm length with average crack spacing between 30 mm and 45 mm, See Table 4).

(a) Interface failure

(b) Substrate failure

Fig. 12 – Failure modes determined from pull-off test

Table 6 – Summary of pull-off test results

Shot-blasted interface				Sand-blasted interface			
No.	P_{max} (kN)	Stress (MPa)	Failed at	No.	P_{max} (kN)	Stress (MPa)	Failed at
1	4.80	2.37	substrate	1	2.10	1.04	interface
2	6.35	3.14	substrate	2	6.33	3.13	substrate
3	n/a	n/a	n/a	3	2.12	1.05	interface
4	6.75	3.33	substrate	4	5.63	2.78	substrate
5	4.92	2.43	interface	5	6.67	3.29	interface
6	4.51	2.23	substrate	6	2.25	1.11	interface
7	6.86	3.39	substrate	7	8.14	4.02	substrate
8	8.65	4.27	interface	8	3.27	1.62	substrate
9	7.04	3.48	substrate	9	8.45	4.17	substrate
10	n/a	n/a	n/a	10	5.86	2.90	substrate
11	6.57	3.24	interface	11	7.04	3.48	substrate
12	6.16	3.04	interface	12	6.24	3.08	substrate
	average	3.09			average	2.64	
	standard deviation	0.62			standard deviation	1.14	
	cov	0.20			cov	0.43	

NOTE: n/a - test results are not available due to adhesive failure.

Table 7 – Design value (characteristic value = average minus one standard deviation, ACI 549.4R-13)

ε_{fk} (%)	f_{fk} (MPa)	E_{fk} (MPa)	f_{isk} (MPa)	f_{bk} (MPa)
3.8	1,282	302	1.25	1.89

In Table 4, the AF tensile stress at the peak load is 1,351 MPa (average of seven tests) with a standard deviation of 69.1 MPa, which results in a characteristic strength of 1,282 MPa. Only 58% of the full AF strength in tension could be realized in the current AF-FRCM system due to slip of AF from the cementitious matrix. Average strain at the peak is 46,480 μm/m with a standard deviation of 8,530 μm/m, which results in a characteristic value of 37,950 μm/m. From tensile test results, tensile modulus of elasticity of the cracked specimen can be evaluated from slope of the line that connects two points at stress levels equal to 0.90 f_{fu} and 0.60 f_{fu} as shown in Eq. (2) as suggested by ACI549.4R-13 [2]:

$$E_f = \frac{\Delta f}{\Delta \varepsilon} = \frac{0.9 f_{fu} - 0.6 f_{fu}}{\varepsilon_{f,09 f_{fu}} - \varepsilon_{f,06 f_{fu}}} \qquad (2)$$

From test results in Table 4 and Fig. 7, E_f is 302 MPa (Average tensile modulus of elasticity of seven tests). It is noted that, unlike other design parameters, an average value was used for the tensile modulus of elasticity.

The interlaminar shear strength of a FRCM system should be considered in case of shear strengthening and the flexural strengthening using the FRCM technology. In this study, the average short beam strength determined using Eq. (2) was 1.30 MPa with a standard deviation of 0.05 MPa, which resulted in 1.25 MPa characteristic strength.

The pull-off test results showed two different failure modes: interface failure in tension and tensile failure in existing concrete (i.e. substrate tensile failure). Overall, the interface strength of the shot-blasted interface was greater than the interface strength of the sand-blasted interface. From all pull-off tests, the average pull-off strength was 2.84 MPa with standard deviation of 0.95 MPa, which results in a design strength of 1.89 MPa. The design values (characteristic strengths) are summarized in Table 7.

5 Conclusions

The research objective was to provide basic design parameters through mechanical characterization of the aramid fiber mesh-green cementitious matrix FRCM system used in this study. Three different types of tests were conducted: Uniaxial test of tensile specimens; flexural test of composite short beams; and pull-off test of FRCM placed on top of normal strength concrete.

(1) The fiber amount (volumetric ratio of the axial AF to gross volume = 0.65%) was adequate such that the fiber tensile behavior governed the tensile behavior of the FRCM system at the peak load.

(2) Relatively ductile tensile behavior with resistance equal to 6.4 MPa in tension (nominal stress) and 4.6% tensile strain at the peak was observed (average of seven tests).

(3) The aramid fiber mesh slipped from the cementitious matrix close to the peak load. This was evidenced by the fact that, although the average strain measured at the peak load was 4.6%, the aramid fibers developed only 58% of the tensile strength at the peak.

(4) The fiber slip could have occurred in two different ways: Slip of internal fiber filaments from the outer fiber filaments in an aramid fiber roving; and slip of the aramid fiber roving from cementitious matrix.

(5) In the flexural test of composite short beams, all failure mode was flexural failure rather than shear failure (such as interface delamination or debonding in the fiber mesh plane). The average short beam strength of seven tests was 1.3 MPa. It is suggested that the interlaminar shear strength is 1.3 MPa or greater.

(6) In the pull-off test, two different failure modes were identified: Interface tensile failure (interface failure) and tensile failure of the existing concrete (substrate failure). Overall, an average pull-off strength of 2.84 MPa was determined (average of 22 tests).

(7) Design parameters for the AF-FRCM system used in this study were suggested. The elastic modulus is low in the AF-FRCM system indicating significant slip of the fibers in the cementitious matrix.

(8) Green high-strength cementitious matrix used in this study developed 75.6 MPa strength after 56 days and developed total shrinkage of 717 micro strain after 90 days. The mortar properties are considered proper for the use in the AF-FRCM system while it is a more economical mix than the conventional mix

Acknowledgement

This research was supported by a grant (20CTAP-C152175-02) from Technology Advancement Research Program (TARP) funded by the Ministry of Land, Infrastructure, and Transport of the Korean government

References

1. Firmo, J.P.; Correia, J.R.; and Bisby, L.A. (2015) "Fire behavior of FRP-strengthened reinforced concrete structural elements: A state-of-the-art review," Composites Part B: Engineering, vol. 80, pp. 198-216.
2. ACI 549.4R (2013) Guide to Design and Construction of Externally-Bonded Fabric-Reinforced Cementitious Matrix (FRCM) Systems for Repair and Strengthening Concrete and Masonry Structures, American Concrete Institute, Farmington Hills, MI.
3. Larbi, A.S.; Agbossou, A.; and Hamelin, P. (2013) "Experimental and numerical investigation about textile-reinforced concrete and hybrid solutions for repairing and/or strengthening reinforced concrete beams," Composite Structures, vol. 99, pp. 152-162.
4. Peled, A.; and Mobasher B. (2007) "Tensile behavior of Fabric Cement-Based Composites: Pultruded and Cast," ASCE Journal of Materials, vol. 19, no. 4, pp. 340-348.
5. Caggegi, C.; Lanoye, E.; Djama, K.; Bassil, A.; and Gabor A. (2017) "Tensile behaviour of a basalt TRM strengthening system: Influence of mortar and reinforcing textile ratios," Composites Part B: Engineering, vol. 130, pp. 90-102.
6. Domini J.; and Corinaldesi V. (2017) "Mechanical characterization of different FRCM systems for structural reinforcement," Construction and Building Materials, vol. 145, pp. 565-575.
7. Ebead, U.; and Younis, A. (2019) "Pull-off characterization of FRCM/Concrete interface," Composites Part B: Engineering, vol. 165, pp. 545-553.
8. Elsanadedy, H.M.; Abbas, H.; Almusallam, T.H.; and Al-Salloum, Y.A. (2019) "Organic versus inorganic composites for bond-critical strengthening applications of RC structures – State-of-the-art review," Composites Part B: Engineering, vol. 174, pp. 106947.
9. Mazzuca, S.; Hadad, H.A.; Ombres, L.; and Nanni, A. (2019) "Mechanical Characterization of Steel-Reinforced Grout for Strengthening of Existing Masonry and Concrete Structures," ASCE Journal of Materials, vol. 31, no. 5, pp. 0019037.
10. Zamir, M.; Sripada, R.; and Peled, A. (2019) "Hybrid fillers in carbon-fabric-reinforced cement-based composites," Cement and Concrete Composites, vol. 98, pp. 113-124.
11. Dong, J.F.; Wang, Q.Y.; and Guan, Z.W. (2012) "Structural behavior of RC beams externally strengthened with FRP sheets under fatigue and monotonic loading," Engineering Structures, vol. 41, pp. 24-33.
12. Baggio, D.; Soudki, K.; and Noel, M. (2014) "Strengthening of shear critical RC beams with various FRP systems," Construction and Building Materials, vol. 66, pp. 634-644.
13. Bournas, D.A.; Pavese, A.; and Tizani W. (2015) "Tensile capacity of FRP anchors in connecting FRP and TRM sheets to concrete," Engineering Structures, vol. 82, pp. 72-81.
14. Gonzales-Libreros, J.H.; Sabau, C.; Sneed, L.H.; Pellegrino, C.; and Sas G. (2017) "State of research on shear strengthening of RC beams with FRCM composites," Construction and Building Materials, vol. 149, pp. 444-458.
15. Al-Gemeel, A.N.; and Zhuge, Y. (2019) "Using textile reinforced engineered cementitious composite for concrete columns confinement," Composite Structures, vol. 210, pp. 695-706.
16. Marcinczak, D.; Trapko, T.; and Musial, M. (2019) "Shear strengthening of reinforced concrete beams with PBO-FRCM composites with anchorage," Composites Part B: Engineering, vol. 158, pp. 149-161.
17. Hadad, H.A.; Erickson, B.; and Nanni, A. (2020) "Flexural analysis and design of FRCM-strengthened RC beams," Construction and Building Materials, vol. 244, pp. 118371.
18. Raoof, S.M.; and Bournas, D.A. (2017) "TRM versus FRP in flexural strengthening of RC beams: behavior at high temperatures," Construction and Building Materials, vol. 154, pp. 424-437.
19. Messori, M.; Nobili, A.; Signorini, C.; and Sola A. (2019) "Effect of high temperature exposure on epoxy-coated glass textile reinforced mortar (GTRM) composites," Construction and Building Materials, vol. 212, pp. 765-774.
20. Ebead, U.; and El-Sherif, H. (2019) "Near surface embedded-FRCM for flexural strengthening of reinforced concrete beams," Construction and Building Materials, vol. 204, pp. 166-176.
21. Carozzi, F.G.; Poggi, C.; Bertolesi, E.; Milani, G. (2018) "Ancient masonry arches and vaults strengthened with TRM, SRG and FRP composites: Experimental evaluation," Composite Structures, vol. 187, pp. 466-480.
22. Caggegi, C.; Carrozi, F.G.; Santis, S.D.; Fabbrocino, F.; Focacci, F.; Hojdys, L.; Lanoye, E.; and Zuccarino, L. (2017) "Experimental analysis on tensile and bond properties of PBO and

aramid fabric reinforced cementitious matrix for strengthening masonry structures," Composites Part B: Engineering, vol. 127, pp. 175-195.
23. Ascione, L.; De Felice, G.; and De Santis, S. (2015) "A qualification method for externally bonded Fibre Reinforced Cementitious Matrix (FRCM) strengthening systems," Composite Part B: Engineering, vol. 78: pp. 497-506.
24. ASTM D2344M (2016) Standard Test Method for Short-Beam Strength of Polymer Matrix Composite Materials and Their Laminates, ASTM International, West Conshohocken, PA.
25. ISO 10406-2 (2015) Fibre-reinforced polymer (FRP) reinforcement of concrete – test methods – Part 2: FRP sheets, Geneva, Switzerland.
26. Choi, D.-U.; Fowler, D.W.; and Wheat, D.L. (1996) "Thermal Stresses in Polymer Concrete Overlays," American Concrete Institute, Special Publication SP-166, Properties and Uses of Polymers in Concrete, pp. 93-122.
27. Soliman, N.A.; and Tagnit-Hamou, A. (2017) "Partial substitution of silica fume with fine glass powder in UHPC: Filling the micro gap," Construction and Building Materials, vol. 139, pp. 374-383.
28. KS L 5105 (2007) Testing method for compressive strength of hydraulic mortar, Korean Agency for Technology and Standards (KATS).
29. ASTM D642 (2013) Standard Test Method for Density, Absorption, and Voids in Hardened concrete, ASTM International, West Conshohocken, PA.
30. KS F 2527 (2018) Concrete aggregates, Korean Agency for Technology and Standards (KATS).
31. Chinzorigt, G.; Lim, M.K.; Yu, M.; Lee, H.; Enkbold, O.; and Choi, D. (2020) "Strength, shrinkage and creep and durability aspects of concrete including CO_2 treated recycled fine aggregate," Cement and Concrete research, vol. 136, pp. 106062.
32. ASTM STP763, Measuring Surface Texture by the Sand-Patch Method, ASTM International, West Conshohocken, PA.
33. ACI 209R (1992) Prediction of Creep, Shrinkage, and Temperature Effects in Concrete Structures, American Concrete Institute, Farmington Hills, MI.